DOI: 10.1002/ejic.200800480

Erbium-Complex-Doped Near-Infrared Luminescent and Magnetic Macroporous Materials

Wei-Qiang Fan,[a–c] Jing Feng,[a–c] Shu-Yan Song,[a–c] Yong-Qian Lei,[a–c] Yan Xing,[a] Rui-Ping Deng,[a–c] Song Dang,[a–c] and Hong-Jie Zhang*[a]

Keywords: Macroporous materials / Near-infrared luminescence / Magnetism

A near-infrared luminescent macroporous material (PL–Macromaterial) and a near-infrared luminescent/magnetic bifunctional macroporous material (M/PL–Macromaterial) were synthesized by using polystyrene microspheres (PS) and Fe_3O_4@polystyrene core–shell nanoparticles (Fe_3O_4@PS), respectively, as templates. Both the PL–Macromaterial and the M/PL–Macromaterial show the characteristic emission of the Er^{3+} ion. Moreover, the M/PL–Macromaterial possesses superparamagnetic properties at room temperature. The photoluminescence, magnetism, and macroporous morphologies of the macroporous materals were investigated.

Introduction

Macroporous materials, which are prepared with colloid crystals as templates, possess pores that are larger than ca. 50 nm in diameter. The pores of the macroporous materials interconnect with each other through a small windows.[1] Recently, templating by opaline lattice assemblies generating macroporous materials has attracted much attention, because of applications in photonic crystals,[2] catalysis,[3] magnetics,[4] and photoluminescence.[5] But comparatively little is known on lanthanide-complex-doped optical macroporous materials, and to combine multiple compositions and functions within one macroporous material is perhaps very interesting.[6]

Our group has made some efforts towards the study of mesoporous silica materials doped with lanthanide complexes, and a series of visible and near-infrared luminescent hybrid mesoporous materials have been obtained.[7–9] Mesoporous materials possessing an inert host matrix, which will be available to be doped or grafted with lanthanide complexes, can improve the photo- and thermal stabilities of the lanthanide complexes. Compared with mesoporous materials, macroporous materials have the following advantages:[10–14] (a) a macroporous structure can be a beneficial host for chemical species too large for mesoporous materials; (b) 3D-ordered macroporous materials (3DOM) have photonic stop bands and have potential applications in optical waveguides, optical circuits, and low-threshold telecommunications lasers; (c) core–shell colloid crystals can be chosen as templates, and cores can remain behind in the sphere pores after removing the templates, which can add new functionality to the obtained macroporous materials.

Furthermore, if luminescent dyes are incorporated into the 3DOM structure, or the 3DOM structure exhibits intrinsic luminescence, overlaps between stop bands and emission bands can be used to suppress the luminescence in a controlled manner.[15] Lanthanide complexes, which exhibit very efficient emission under ultraviolet excitation, are a useful class of luminophores.[16] Especially, erbium-doped materials show the characteristic emission of the Er^{3+} ion originating from an intra-4f shell transition from its first excited state ($^4I_{13/2}$) to the ground state ($^4I_{15/2}$), which locates at the third telecommunication window. Thus, macroporous materials doped with erbium complexes will possess outstanding near-infrared luminescence for further optical study in 3DOM structures. In order to improve the thermal stability of the lanthanide complexes in the macroporous materials, we used the SiO_2 sol of lanthanide complexes as precursors. Macroporous materials will integrate both the magnetic and optical property functionalities into a single construction if they are produced by combining the magnetic core–shell colloid crystal with lanthanide complex sol precursors. Moreover, bifunctional materials with both magnetic and optical properties have recently become a class of intriguing materials to be studied.[17]

The complexes of the rare-earth ions with β-diketonates, aromatic carboxylic acids, and heterocyclic ligands containing nitrogen hardly dissolved in the sol–gel solution, so we used in situ synthetic methods, which are useful for intro-

[a] State Key Laboratory of Rare Earth Resource Utilizations, Changchun Institute of Applied Chemistry
Changchun 130022, P. R. China
Fax: +86-431-85698041
E-mail: hongjie@ciac.jl.cn
[b] Chinese Academy of Sciences
Changchun 130022, P. R. China
[c] Graduate School of the Chinese Academy of Sciences
Beijing, P. R. China

ducing the rare-earth complexes into the sol–gel system, to synthesize a clear Er/DBM/phen/TEOS sol (DBM = dibenzoylmethanate; phen = 1,10-phenanthroline; TEOS = tetraethoxysilane) as the precursor. Furthermore the hybrid organic–inorganic materials that form by in situ synthetic methods are quite uniformly composed and mixed at a molecular level.[18a] We introduced PS and Fe_3O_4@PS as the templates to prepare the macroporous materials PL–Macromaterial and M/PL–Macromaterial, respectively, which were obtained when the polystyrene in the templates was removed by tetrahydrofuran (THF). The Er/DBM/phen complex was synthesized in the macroporous materials, and was verified by FTIR, diffuse reflectance (DR), and photoluminescence spectra. Macroporous materials with near-infrared luminescence and magnetic properties have potential use in amplifiers or planar waveguide materials, adsorption materials for chemical species, and photonic crystals.

Results and Discussion

The steps involving the synthesis of macroporous materials are described in Scheme 1.

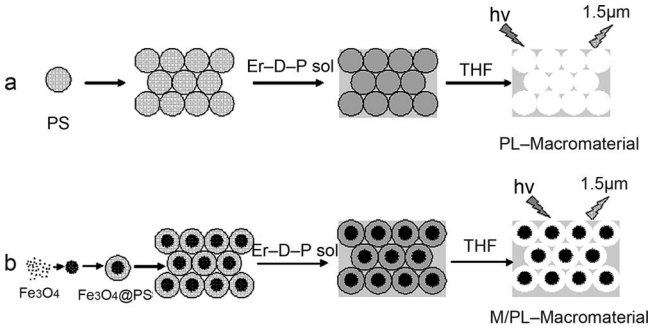

Scheme 1. Synthetic procedures for the PL–Macromaterial (a) and the M/PL–Macromaterial (b).

The PL–Macromaterial was prepared by capillary infiltration of colloidal crystals of about 417-nm-diameter polystyrene nanospheres (Figure 1a) with the Er/DBM/phen/TEOS sol (Er–D–P sol) as the precursor. According to the SEM images (Figure 1b) the PL–Macromaterial formed a thick film of about 12 μm. We can see from the magnified view of the PL–Macromaterial (Figure 1c) that the sample consists of 320-nm-diameter spherical pores that are interconnected through ca. 80-nm-wide apertures and surrounded by a continuous gel framework, which proves that the spherical pores are close-packed and interconnected through apertures. The core–shell structure of the Fe_3O_4@PS nanoparticles is revealed by TEM (Figure 1d). The M/PL–Macromaterial was obtained by using Fe_3O_4@PS core–shell nanoparticles as templates. The thickness of the M/PL–Macromaterial film is about 3 μm (Figure 1e), and on the basis of the SEM images most of the pores contain Fe_3O_4 nanoclusters inside (Figure 1f). The Fe quantitative analysis of the M/PL–Macromaterial was conducted by an energy-dispersive X-ray (EDX) analyzer coupled to the SEM. There is an Fe peak in the EDX spectrum (Figure 1g), which further indicates the presence of Fe_3O_4 nanoclusters in the M/PL–Macromaterial.

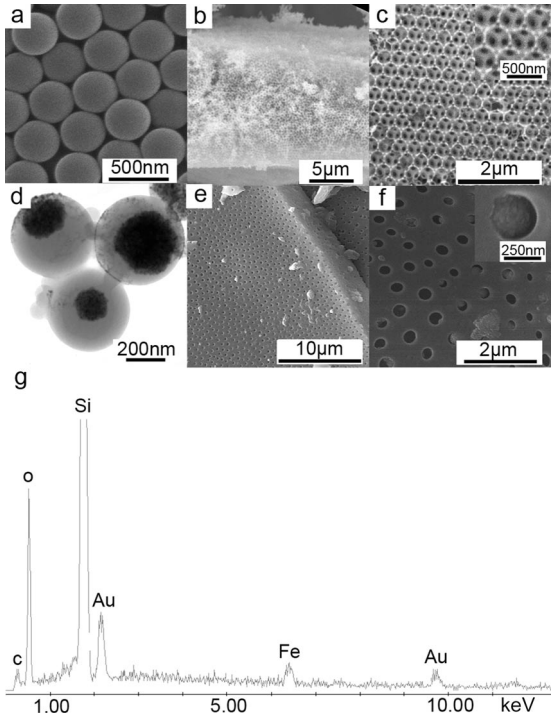

Figure 1. SEM images: PS (a), PL–Macromaterial film (b), magnified view of PL–Macromaterial (c), M/PL–Macromaterial film (e), and magnified view of M/PL–Macromaterial (f). TEM image of Fe_3O_4@PS (d). EDX spectrum of the M/PL–Macromaterial (g).

The components of the framework of the macroporous materials was characterized by FTIR spectroscopy. The IR spectra of the pure $Er(DBM)_3$phen complex, phen/SiO_2 macroporous material, PL–Macromaterial, and M/PL–Macromaterial are shown in Figure 2. For the pure $Er(DBM)_3$phen complex (Figure 2a) both the coordination bonds of Er–phen and Er–DBM are evident by the bands appearing in the range 400–438 cm^{-1}, corresponding to the ν(Er–O) vibration and the peak at 517 cm^{-1} from the ν(Er–N) vibration.[18b] With regard to the IR spectrum of the PL–Macromaterial in Figure 2c, the peak at 1074 cm^{-1} can be attributed to the Si–O–Si symmetric stretching vibration, and the band at 450 cm^{-1} corresponds to the bending vibration of the O–Si–O band.[18c] The stretching vibration frequency of the C=N band in the phen/SiO_2 macroporous material shows a peak at 1640 cm^{-1}. We can also see that the stretching vibration frequency of C=N of phen in the PL–Macromaterial has red-shifted to 1622 cm^{-1}, which suggests the possible coordination of Er–N. Figure 2c shows that a new but weak absorption band appears at 419 cm^{-1} (see inset) that can be assigned to the stretching band of Er–O.[19] The IR spectrum of the M/PL–Macromaterial is similar to that of the PL–Macromaterial, but the stretching band of Er–O is not discernible in Figure 2d. The weak and poorly discernible band of Er–O in the spectra of the samples is probably because of the low concentration of the erbium complex in the samples (Er^{3+}/Si molar ratio =

1:100). From the analysis of the IR spectra above we can suggest that the erbium complex was possibly synthesized in the macroporous materials.

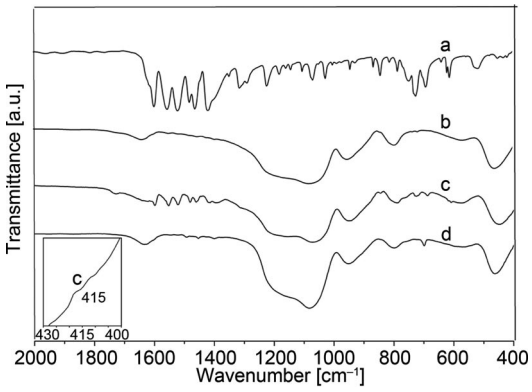

Figure 2. FTIR spectra of the pure $Er(DBM)_3$phen complexes (a), phen/SiO_2 macroporous materials (b), PL–Macromaterial (c), and M/PL–Macromaterial (d).

Figure 3 exhibits the DR spectra of the pure $Er(DBM)_3$-phen complex, PL–Macromaterial, and M/PL–Macromaterial. The ground state to the excited states of the Er^{3+} ions are both observed in Figure 3a, where the peaks at 488, 522, and 652 nm are assigned to $^4I_{15/2}\rightarrow{}^4F_{7/2}$, $^4I_{15/2}\rightarrow{}^2H_{11/2}$, and $^4I_{15/2}\rightarrow{}^4F_{9/2}$, respectively. The absorption peaks of the Er^{3+} ions are very weak in the PL–Macromaterial and M/PL–Macromaterial, which might be because of the low concentration of the erbium complex in the samples. The broad absorption bands from 200 to 400 nm can be attributed to electronic transitions from the ground-state level (π) S_0 to the excited level (π^*) S_1 of the organic ligands, but the broad absorption band of the M/PL–Macromaterial has extended to 500 nm, which may be because of the absorption of iron oxide. In conclusion, the broad ligand-absorption bands are present in the DR spectra of the PL–Macromaterial and M/PL–Macromaterial in comparison with the pure $Er(DBM)_3$phen complex, which also indicates that the erbium complex has been synthesized in situ in the samples.

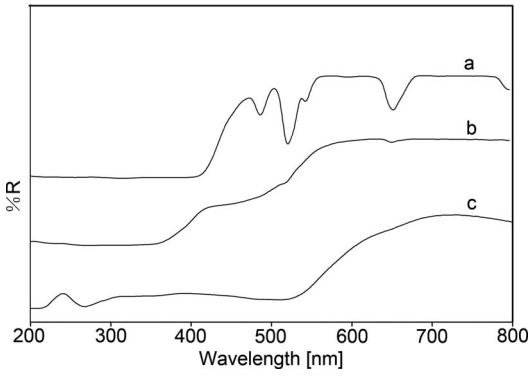

Figure 3. DR spectra of the pure $Er(DBM)_3$phen complex (a), PL–Macromaterial (b), and M/PL–Macromaterial (c).

We then studied the photoluminescence spectra of the samples in order to further verify that the erbium complex is synthesized in the samples. Figure 4 shows the excitation spectra of the macroporous materials and the absorption spectra of the DBM (Figure 4c) and phen (Figure 4d) ligands. There are overlaps between the excitation bands of the macroporous materials and the absorption bands of the DBM and phen ligands, which indicates the typical sensitization of the Er^{3+} ions by the two organic ligands, and thus indirectly confirms that the Er^{3+} ions have formed the erbium complex with the DBM and phen ligands in both the PL–Macromaterial and the M/PL–Macromaterial. In the excitation spectra the broad band from 250 to 450 nm may be a result of the absorption of the organic ligands, which agrees with the DR spectra. In Figure 5, ligand-mediated excitation at 390 and 393 nm in the emission spectra of the PL–Macromaterial and M/PL–Macromaterial, respectively, clearly shows the emission bands centered at 1530 nm. The emission bands extend from 1436 to 1640 nm and from 1450 to 1640 nm for the PL–Macromaterial and M/PL–Macromaterial, respectively. The emission around 1530 nm can be attributed to the transition from the first excited state ($^4I_{13/2}$) to the ground state ($^4I_{15/2}$) of the Er^{3+} ions. This indicates that the energy transfers from the ligands to the Er^{3+} ions, which provides further evidence that the erbium complex has formed in the macroporous materials.

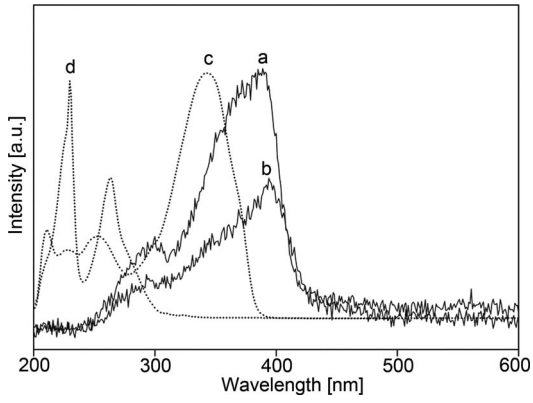

Figure 4. Excitation spectra of the PL–Macromaterial (λ_{em} = 1530 nm) (a) and M/PL–Macromaterial (λ_{em} = 1530 nm) (b). UV/Vis absorption spectra of DBM (c) and phen (d).

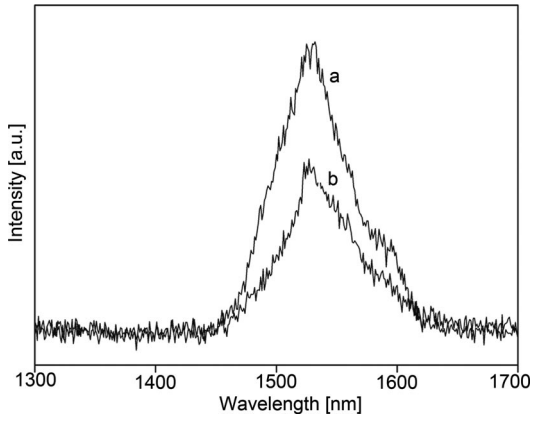

Figure 5. Emission spectra of the PL–Macromaterial (λ_{ex} = 390 nm) (a) and M/PL–Macromaterial (λ_{ex} = 393 nm) (b).

Recently, there has been an urgent demand for optical amplifiers with a wide- and flat-gain spectrum in the telecommunication window because of the rapid increase of information capacity. The transition from $^4I_{13/2}$ to $^4I_{15/2}$ of the Er^{3+} ion is in the right position of the third telecommunication window. Therefore, materials with a wide 1.5-μm emission bandwidth of Er^{3+} ions have attracted considerable attention.[20] However, the full width at half maximum (fwhm) of the erbium-doped inorganic material is relatively small, so erbium–organic compounds that show broadband 1.5-μm emissions have been intensively studied.[7,19,21] The fwhm of the $^4I_{13/2}\rightarrow{}^4I_{15/2}$ transition for the PL–Macromaterial is 1.389×10^5 cm^{-1} (72 nm), and the fwhm for the M/PL–Macromaterial is 1.3667×10^5 cm^{-1} (61 nm). Such relatively broad spectra may enable a wide-gain bandwidth for optical amplification. Therefore, the macroporous materials with the characteristic emission of the Er^{3+} ions may offer the opportunity to develop new materials suitable for optical amplifiers.

The magnetic properties of the M/PL–Macromaterial were characterized by using a superconducting quantum interference device (SQUID) magnetometer with fields of up to 5 T. As shown in Figure 6a, the M/PL–Macromaterial exhibits no magnetic hysteresis for the magnetization curves at room temperature. This is characteristic of superparamagnetic nanoparticles, in which thermal fluctuations are sufficient to overcome the anisotropic energy barrier.[17b]

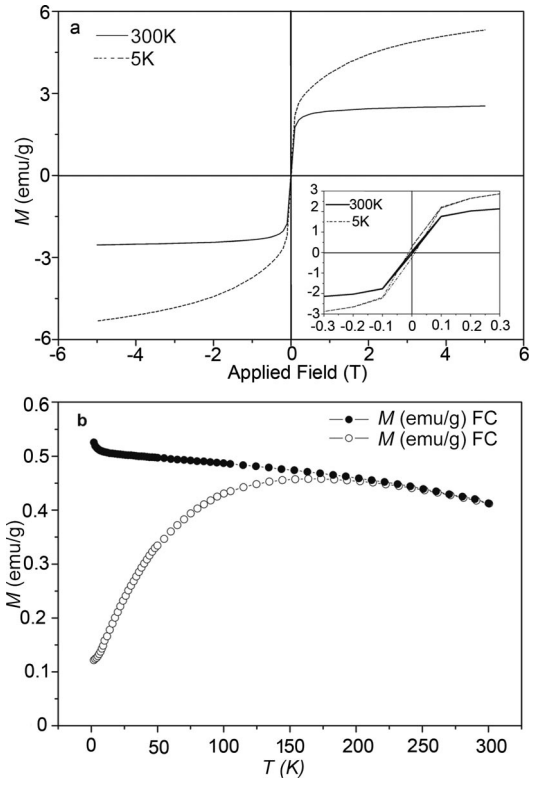

Figure 6. Magnetization curves measured at 300 and 5 K (a), and zero-field-cooled (ZFC) and field-cooled (FC) magnetization curves of the M/PL–Macromaterial at 100 Oe (b). The inset in plot (a) is a magnified view of the magnetization curves at low applied fields.

The magnetic properties of Fe_3O_4 nanoparticles prepared by coprecipitation methods exhibit superparamagnetic behavior at room temperature, which has been reported previously.[22a] The superparamagnetic behavior was still retained when the Fe_3O_4 nanoparticles aggregated into clusters in the pores of the sample, which are believed to be derived from the dispersed magnetite-nanoparticle clusters among the pores of the M/PL–Macromaterial.

The saturation magnetization of the M/PL–Macromaterial at room temperature reaches a saturation moment of 2.53 emu/g. This low saturation magnetization can be attributed to the increased distance between the magnetic nanoclusters separated by hybrid gel walls in the macroporous material. The temperature dependence of the zero-field-cooled and field-cooled (ZFC/FC) magnetization is shown in Figure 6b. The two curves coincide at a high temperature and begin to separate as the temperature decreases; the ZFC curve has a maximum (a characteristic of superparamagnetism)[22b] with a T_B value of about 170 K. Indeed, we observed a magnetic hysteresis loop at 5 K with coercivity (Hc = 115 Oe) and remanence. This bifunctional M/PL–Macromaterial is of particular interest because its properties may be tuned by the application of external stimuli.

Conclusions

In this paper, we have synthesized the near-infrared luminescent PL–Macromaterial and near-infrared luminescent/magnetic bifunctional M/PL–Macromaterial by using PS and Fe_3O_4@PS nanoparticles, respectively, as templates. Both the PL–Macromaterial and M/PL–Macromaterial show the characteristic emission of the Er^{3+} ions originating from an intra-4f shell transition from its first excited state ($^4I_{13/2}$) to the ground state ($^4I_{15/2}$), which locates at the third telecommunication window (centered at 1540 nm). The characteristic emission of the Er^{3+} ions from the macroporous materials indicates the existence of intramolecular energy transfer from the ligands to the Er^{3+} ions. Besides luminescence, this magnetic M/PL–Macromaterial may endow the near-infrared materials with the capacity to respond to magnetic fields.

Experimental Section

General: All chemicals were of reagent grade and were used as commercially obtained.

Synthesis of Surfactant-Free Polystyrene (PS) Spheres: Monodisperse polystyrene spheres were synthesized by using an emulsifier-free emulsion polymerization technique according to the literature.[23,24] The styrene was washed prior to use thrice with 0.1 M NaOH aqueous solution and deionized water. The persulfate solution (20 mg of potassium persulfate dissolved in 20 mL of deionised water) was added to a round-bottomed flask containing the mixture of deionised water (60 mL) and washed styrene (3 mL) at 70 °C, and then the resulting mixture was stirred mechanically for

28 h. The entire procedure was performed under N_2. The PS spheres were collected by centrifugation and finally dispersed in ethanol. We adopted the vertical lifting deposition method to form a film of PS spheres on the glass substrate; first immerse the glass substrate into the ethanol containing the PS spheres, and then vertically lift the glass substrate slowly. In order to obtain a thick film we increased the PS sphere concentration in suspension, and repeatedly immersed and lifted the glass substrate several times.

Synthesis of Fe_3O_4@PS Core–Shell Spheres: Under the protection of N_2, $FeCl_3·6H_2O$ (12 g) and $FeSO_4·7H_2O$ (6.87 g) were dissolved in deionized water (50 mL) under mechanical stirring at 80 °C. Ammonium hydroxide (25 mL) was then rapidly added to the solution. The color of the solution turned black immediately. After 30 min, oleic acid (1.88 g) was then added to the reaction solution, and the mixture was stirred for 1.5 h. The magnetite nanoparticles were washed with deionized water until reaching a neutral pH. The organic ferrofluid was obtained by transferring Fe_3O_4 nanoparticles into the octane solution.[25] SDS (sodium dodecylsulfate) (0.045 g) was dissolved in deionised water (80 mL) and ferrofluid (2 g) was dispersed in the solution by ultrasound. This was followed by the addition of washed styrene (3 mL) to the mixture. A persulfate solution (20 mg of potassium persulfate dissolved in 20 mL of deionised water) was added to the reaction flask at 70 °C. The whole mixture was stirred at a specific stirring speed for 28 h, and the reactor was kept under N_2. Fe_3O_4@PS core–shell spheres were collected by magnets, and the film of Fe_3O_4@PS spheres on the glass substrate was achieved by the same method mentioned above.

Synthesis of Macroporous Materials: The Er–D–P sol was prepared by an in situ synthetic method according to the literature.[19] The molar ratio of TEOS/ethanol/deionized water (acidified with HCl) in the starting solution was 1:4:4. The resulting clear sol, with a pH of about 2.5, was stirred for 2 h. DBM, phen, and $ErCl_3$, all in ethanol, were then introduced consecutively into the starting solution. The molar ratio of Er/DBM/phen was 1:3:1 (Er/TEOS molar ratio: 1:100), and the solution was stirred in a sealed plastic container for 2 h. It is worth noting that the concentration of the erbium complex cannot be increased because a high concentration will result in deposition in the sol. The films of PS spheres and Fe_3O_4@PS spheres on the glass substrates were immersed into the Er–D–P sol and kept for 4 h, and then the glass substrates were taken out of the sol and dried at room temperature. The polystyrene part of the templates was removed by THF, and the remaining parts are the PL–Macromaterial and M/PL–Macromaterial, respectively.

Characterization: The morphologies and structures of the products were characterized by field-emission scanning electron microscopy (FESEM) and transmission electron microscopy (TEM). FESEM analysis was conducted with a Philips XL-30 field-emission scanning electron microscope operated at 15 kV, whereas TEM observation was carried out with a JEOL-JEM-2010 instrument at 200 kV. Room-temperature photoluminescence spectra were recorded with a Fluorolog-3 using a 450-W xenon lamp as the excitation source at room temperature. The UV/Vis absorption spectra of DBM and phen were recorded with a TU-1901 spectrophotometer by using ethanol as solvent. FTIR spectra were measured within the 4000–400 cm^{-1} region with an American BIO-RAD Company model FTS135 infrared spectrophotometer by using the KBr pellet technique. DR spectra were measured with a Shimadzu UV-3600 spectrophotometer. The magnetic characterizations of the M/PL–Macromaterial were performed with a superconducting quantum interference device (SQUID) magnetometer with fields of up to 5 T.

Acknowledgments

The authors are grateful to the financial aid from the National Natural Science Foundation of China (Grant No.: 20631040) and the MOST of China (Grant No.: 2006CB601103).

[1] a) Y. Xia, Y. Lu, K. Kamata, B. Gates, Y. Yin, "Macroporous Materials Containing Three-Dimensionally Periodic Structures" in *Chemistry of Nanostructured Materials* (Ed.: P. Yang), World Scientific, Singapore, **2003**, pp. 69–100; b) T. H. Brian, C. F. Blanford, A. Stein, *Science* **1998**, *281*, 538–540; c) P. Yang, T. Deng, D. Zhao, P. Feng, D. Pine, B. F. Chmelkal, G. M. Whitesides, G. D. Stucky, *Science* **1998**, *282*, 2244–2246.
[2] a) I. Soten, H. Miguez, S. M. Yang, S. Petrov, N. Coombs, N. Tetreault, N. Matsuura, H. E. Ruda, G. A. Ozin, *Adv. Funct. Mater.* **2002**, *12*, 71–77; b) P. D. Yang, A. H. Rizvi, B. Messer, B. F. Chmelka, G. M. Whitesides, G. D. Stucky, *Adv. Mater.* **2001**, *13*, 427–431; c) Y. A. Vlasov, N. Yao, D. J. Norris, *Adv. Mater.* **1999**, *11*, 165–169.
[3] C. Wang, A. Geng, Y. Guo, S. Jiang, X. Qu, *Mater. Lett.* **2006**, *60*, 2711–2714.
[4] a) Y. N. Kim, S. J. Kim, E. K. Lee, E. O. Chi, N. H. Hur, C. S. Hong, *J. Mater. Chem.* **2004**, *14*, 1774–1777; b) J. Gallery, M. Ginzburg, H. Miguez, S. M. Yang, N. Coombs, A. Safa-Sefat, J. E. Greedan, I. Manners, G. A. Ozin, *Adv. Funct. Mater.* **2002**, *12*, 382–388.
[5] a) Y. Liu, S. Wang, *Colloids Surf. B* **2007**, *58*, 8–13; b) R. Withnall, T. G. Ireland, M. I. Martinez-Rubio, G. R. Fern, J. Silver, *J. Mod. Opt.* **2002**, *49*, 965–976; c) A. Ghadimi, L. Cademartiri, U. Kamp, G. A. Ozin, *Nano Lett.* **2007**, *7*, 3864–3868.
[6] A. Stein, *Microporous Mesoporous Mater.* **2001**, *44–45*, 227–239.
[7] L. N. Sun, H. J. Zhang, C. Y. Peng, J. B. Yu, Q. G. Meng, L. S. Fu, F. Y. Liu, X. M. Guo, *J. Phys. Chem. B* **2006**, *110*, 7249–7258.
[8] a) H. R. Li, J. Lin, H. J. Zhang, H. C. Li, L. S. Fu, Q. G. Meng, *Chem. Commun.* **2001**, 1212–1213; b) H. R. Li, J. Lin, H. J. Zhang, L. S. Fu, Q. G. Meng, S. B. Wang, *Chem. Mater.* **2002**, *14*, 3651–3655; c) Q. G. Meng, P. Boutinaud, A. C. Franville, H. J. Zhang, R. Mahiou, *Microporous Mesoporous Mater.* **2003**, *65*, 127–136.
[9] C. Y. Peng, H. J. Zhang, J. B. Yu, Q. G. Meng, L. S. Fu, H. R. Li, L. N. Sun, X. M. Guo, *J. Phys. Chem. B* **2005**, *109*, 15278–15287.
[10] R. C. Schroden, A. Stein, "3D Ordered Macroporous Materials" in *Colloids and Colloid Assemblies* (Ed.: F. Caruso), Wiley-VCH, Weinheim, Germany, **2004**, pp. 465–493.
[11] E. Yablonovitch, *J. Opt. Soc. Am. B* **1993**, *10*, 283–295.
[12] J. D. Joannopoulos, P. R. Villeneuve, S. Fan, *Nature* **1997**, *386*, 143–149.
[13] S. Y. Lin, E. Chow, V. Hietala, P. R. Villeneuve, J. D. Joannopoulos, *Science* **1998**, *282*, 274–276.
[14] a) Y. Lu, Y. Yin, Y. Xia, *Nano Lett.* **2002**, *2*, 785–788; b) B. Rodriguez-Gonzalez, V. Salgueirino-Maceria, F. Garcia-Santamaria, L. M. Liz-Marzan, *Nano Lett.* **2002**, *2*, 471–473.
[15] a) A. Stein, R. C. Schroden, *Curr. Opin. Solid State Mater. Sci.* **2001**, *5*, 553–564; b) A. C. Arsenault, T. J. Clark, G. von Freymann, L. Cademartiri, R. Sapienza, J. Bertolotti, E. Vekris, S. Wong, V. Kitaev, I. Manners, R. Z. Wang, S. John, D. Wiersma, G. A. Ozin, *Nat. Mater.* **2006**, *5*, 179–184; c) H. P. Schriemer, H. M. van Driel, A. F. Koenderink, W. L. Vos, *Phys. Rev. A* **2000**, *63*, 011801-1–011801-4.
[16] a) X. M. Guo, L. S. Fu, H. J. Zhang, L. D. Carlos, C. Y. Peng, J. F. Guo, J. B. Yu, R. P. Deng, L. N. Sun, *New J. Chem.* **2005**, *29*, 1351–1358; b) S. Gago, J. A. Fernandes, J. P. Rainho, R. A. SáFerreira, M. Pillinger, A. A. Valente, T. M. Santos, L. D. Carlos, P. J. A. Ribeiro-Claro, I. S. Goncüalves, *Chem. Mater.* **2005**, *17*, 5077–5084; c) P. C. R. Soares-Santos, H. I. S. Nogueira, V. Felix, M. G. B. Drew, R. A. S. Ferreira, L. D. Carlos,

T. Trindade, *Chem. Mater.* **2003**, *15*, 100–108; d) R. A. SáFerreira, L. D. Carlos, R. R. Gonçalves, S. J. L. Ribeiro, V. de Zea Bermudez, *Chem. Mater.* **2001**, *13*, 2991–2998.

[17] a) B. V. Harbuzaru, A. Corma, F. Rey, P. Atienzar, J. L. Jordá, H. García, D. Ananias, L. D. Carlos, J. Rocha, *Angew. Chem. Int. Ed.* **2008**, *120*, 1096–1099; b) S. Y. Yu, H. J. Zhang, J. B. Yu, C. Wang, L. N. Sun, W. D. Shi, *Langmuir* **2007**, *23*, 7836–7840.

[18] a) S. Dang, L. N. Sun, H. J. Zhang, X. M. Guo, Z. F. Li, J. Feng, H. D. Guo, Z. Y. Guo, *J. Phys. Chem. C* **2008**, *112*, 13240–13247; b) L. J. Bian, H. A. Xi, X. F. Qian, J. Yin, Z. K. Zhu, Q. H. Lu, *Mater. Res. Bull.* **2002**, *37*, 2293–2301; c) H. R. Li, H. J. Zhang, J. Lin, S. B. Wang, K. Y. Yang, *J. Non-Cryst. Solids* **2000**, *278*, 218–222.

[19] L. N. Sun, H. J. Zhang, L. S. Fu, F. Y. Liu, Q. G. Meng, C. Y. Peng, J. B. Yu, *Adv. Funct. Mater.* **2005**, *15*, 1041–1048.

[20] a) J. T. Sun, J. H. Zhang, Y. S. Luo, J. L. Lin, H. W. Song, *J. Appl. Phys.* **2003**, *94*, 1325–1328; b) A. Jha, S. Shen, M. Naftaly, *Phys. Rev. B* **2000**, *62*, 6215–6227.

[21] a) O. H. Park, S. Y. Seo, B. S. Bae, J. H. Shin, *Appl. Phys. Lett.* **2003**, *82*, 2787–2789; b) O. H. Park, S. Y. Seo, J. I. Jung, J. Y. Bae, B. S. Bae, *J. Mater. Res.* **2003**, *18*, 1039–1042.

[22] a) L. H. Zhang, B. F. Liu, S. J. Dong, *J. Phys. Chem. B* **2007**, *111*, 10448–10452; b) S. Morup, F. Bodker, P. V. Hendriksen, S. Linderoth, *Phys. Rev. B* **1995**, *52*, 287–294.

[23] T. Sen, G. J. T. Tiddy, J. L. Casci, M. W. Anderson, *Angew. Chem. Int. Ed.* **2003**, *42*, 4649–4653.

[24] B. T. Holland, C. F. Blanford, T. Do, A. Stein, *Chem. Mater.* **1999**, *11*, 795–805.

[25] H. Xu, L. Cui, N. Tong, H. Gu, *J. Am. Chem. Soc.* **2006**, *128*, 15582–15583.

Received: May 14, 2008
Published Online: November 5, 2008

